Reconfigurable Intelligent Surface and UAV–Assisted THz Mobile Communications

Sara Farrag
German University in Cairo
sarah.farrag@guc.edu.eg

Engy Maher
German University in Cairo
engy.maher@guc.edu.eg

Ahmed El-Mahdy
German University in Cairo
ahmed.elmahdy@guc.edu.eg

Falko Dressler
TU Berlin
dressler@ccs-labs.org

***Abstract*—Terahertz (THz) Communications are promising candidate for achieving ultra high data rate suitable for 5G and beyond. Unmanned Aerial Vehicle (UAV) is an emerging facility that can be utilized to assist wireless communications. A reconfigurable intelligent surface (RIS) is deployed such that the phase shifts of its elements are reconfigured to create favorable beam steering, which in turn mitigates undesired interference from other existing links in the network. In this paper, we consider a UAV equipped with an RIS operating in THz, where a cellular user link, in addition to a number of Device–to–Device (D2D) pairs links are considered. The direct paths between each two communicating nodes are considered as well as the RIS-reflected paths. Then, the sum rate is derived under this scenario. Accordingly, a joint power allocation and phase shifts optimization scheme is proposed for the sake of maximizing the sum rate. The proposed joint power allocation and phase shifts optimization scheme is evaluated in terms of the achieved sum rate. Numerical results show that the proposed scheme surpasses three other schemes, achieving the highest sum rate among them all, under varying different parameters in the network.**

***Index Terms*—Wireless communication, UAV, Terahertz, D2D, RIS, Power optimization, Discrete phase shifts**

I. Introduction

With 4.66 billion active internet users worldwide and the availability of ultra high-speed internet access, the amount of data produced daily surpasses the imagination. It is worth mentioning that by the end of 2021, the volume of data created everyday is measured to be 1.134 trillion MB [1]. Accordingly, carrier frequencies utilized recently for wireless communications have been continuously increasing to suit for the dramatically increasing required bandwidth [2]. In turn, the engineering community exerts great efforts to develop the wide radio bands such as the millimeter-wave (mmW) frequencies and THz for the sake of fulfilling the proportional increase of mobile data demand and pave the way for the future sixth generation (6G) wireless communication systems. The THz frequency band, ranging from 0.1 THz to 10 THz and allocated between radio and optical signals, was the last gap in the spectrum to be bridged. It is worth mentioning that the late discovery of the THz gap and the unknown features of its behavior slowed down the evolution of the THz frequency band in today's wireless networks [2].

Nevertheless, this status is rapidly changing today and THz frequency is currently a promising new research field for telecommunication. This is mainly because of its promising high data rate and capacity compared to traditional RF communication [3]. This achieved capacity is urgently demanded for the escalating requirement of wireless data throughput and proliferation of multimedia platforms. In addition, THz beams are exceptionally narrow to overcome the severe signal loss and attenuation, which in turn makes it difficult for eavesdropping, allowing secure data transmission for military applications. Furthermore, THz waves are also characterized by its high resolution and directivity. Moreover, the THz waves are suitable nominees for uplink communication as they allow non-line-of-sight (NLOS) propagation and are deployed as reliable substitutes in severe weather conditions such as fog, turbulence and rain [4]. At the same time, tremendous challenges exist for commercialization of THz wireless communications. For instance, compared to lower-frequency communication systems, THz signals experience more attenuation due to free-space path loss and molecular absorption from atmospheric particles like H_2O. As a solution, high-gain directional antennas or antenna arrays are often deployed for reliable THz systems [5].

Direct D2D is an encouraging technique for users that are physically close to each other. They can communicate directly without referring to the base station (BS). Due to the short distance between each D2D pair, energy consumption is reduced and users' quality of service (QoS) demands are upgraded. Practically, D2D communication is granted the same uplink spectrum as cellular users, which makes the most use of the available bandwidth. Nevertheless, the mitigation of interference arising from D2D communication is innegligible must be highly considered to meet the strict QoS requirements [6]. One of the solutions for this unavoidable interference in networks deploying D2D devices is the deployment of RIS which is considered a key for enabling technologies in 6G [7].

RIS is a 2–dimensional ultra thin reflecting surface along with an integrated electronic circuits. It is composed of a number of elements that can be programmably controlled using varactor diodes. For each of its adaptive elements,

This work is supported by the DAAD and in part by the Federal Ministry of Education and Research (BMBF, Germany) within the 6G Research and Innovation Cluster 6G-RIC under Grant 16KISK020K, in co-operation between the department of telecommunications systems at TU Berlin and German University in Cairo.

the electromagnetic response such as phase shifts towards incident waves can be adaptively altered in a software connected system [8]. Due to the RIS elements' adaptability, the phase shifts of the incident signals are reconfigured to provide a favorable beam steering towards user of interest and remarkably control multi-path effects to satisfy QoS requirements. Compared to conventional amplify and forward (AM) and massive multiple–input–multiple–output (MIMO), RIS forwards much more efficient phase–shifted version of the incident signal. The most distinctive advantage of RIS over AM and MIMO is that the array architecture is passive. In other words, it is operated to reflect rather than to generate. Hence, it is much more power-saving approach since no radio frequency encoding, decoding or power consumption is needed. Through tuning the amplitude and/or phase shifts of the reconfigurable array elements, the received intended power gain is boosted and mitigating interference is destructive [9]. Wireless communication systems that deploy UAVs promise to achieve low–cost wireless connectivity for devices without the need for deploying infrastructure coverage [10]. Compared to terrestrial communications, on–demand wireless systems with low –altitude UAVs are characterized by their speed, flexibility, mobility and are more likely to have better communication channels. This is mainly because of the UAVs that promise higher probability of short-range line-of-sight (LOS) links.

Recently, one of the most emerging UAV applications is UAV relaying in which the UAV is employed in the network to achieve wireless connectivity between two terminals without the existence of direct communication link between them [11]. This certain application is verified as an effective technique to increase throughput, improve reliability and extend BS coverage. Compared to traditional static relays, the UAV-relay is more cost-efficient and has a much higher degree of freedom that is urgently required in rescue operations as well as emergency situations [12]. This motivates us to investigate the performance of the UAV-aided mobile terminals in the presence of interference.

In this paper, we tackle this not-yet investigated point, where the sum rate of the communication link of an uplink RIS-aided network is considered. In our system, one cellular link as well as a number of D2D links are established through a reflected path supported by RIS as well as direct path between each two communicating nodes. In such system, the RIS is deployed on a UAV for higher possibility of THz LOS to enhance the received gain in the presence of interference. The transmitting powers of each transmitting node is optimized as well as the RIS phase shifts.

Our main contributions can be summarized as follows:

- A UAV equipped with an RIS aided network in THz band is considered. A cellular user link and a number of D2D links are transmitted through reflected paths supported by RIS as well as direct paths between each two communicating nodes. Accordingly, the transmitting power of each transmitting node as well as the phase shifts of the RIS reconfigurable elements are studied.
- The sum rate of the scenario under consideration is derived accordingly and it is formulated as a non-convex non-linear mixed integer problem. The constraints for the maximum available power budget, minimum SINR satisfying QoS and the phase shifts are obtained.
- A joint power allocation and phase shifts optimization scheme is proposed to maximize the sum rate of the scenario under consideration. Since the transmitting powers and phase shifts are independent of each other, we decouple the optimization problem into two sub-problems: the transmitting power allocation sub-problem and phase shifts optimization sub-problem.
- For the transmitting power allocation sub-problem, it is solved using difference of concave functions (DC) programming as well as Taylor's expansion. For the phase shifts optimization sub-problem, it is solved using a reasonable-complexity local search algorithm to find the most optimum values of phase shifts.
- Simulations are performed and numerical values are obtained to compare our proposed scheme with other scheme from the literature. The proposed scheme is proven to outperform its counterparts from the literature, achieving higher sum rates in different scenarios.

II. Related Work

There are some works in the literature deploying RIS-aided networks [13], [14]. In [13], the secrecy performance of an RIS-assisted communication network in the presence of an eavesdropping user is investigated. Asympototic analysis of the effect of the number of reflectors deployed in the RIS on the secrecy performance is provided. Simulations illustrates the added-value of deploying RIS to enhance the wireless system secrecy performance. The authors in[14] deployed RIS in a cell-free network. Descent algorithm is deployed and numerical results verify that the energy efficiency of RIS - cell free networks is greatly improved, showing the benefit of deploying RISs.

The most superior feature of THz communications lies in its potential to assist mobile communications at the access level as well as the device level in D2D and drone-to-drone communications. There are handful papers that deploy UAV communication over the THz channel[15], [16], [17]. The authors in [15] analyzed the coverage probability and the area spectral density in a UAV-assisted networks in the THz band. Simulations and numerical results conclude that the coverage probability of the network first increases when increasing the THz UAV BS density and then decreases beyond the maximum. The authors in[16] investigated the challenges in employing high data rate and low latency infrastructure-less wireless UAVs networking in mmWave as well as THz-band communications. The effects of mobile uncertainties on mmWave and THz bands is mainly studied.

From the above discussions, it is concluded that researchers did not yet investigate the sum rate maximization problem

of an uplink RIS-aided network, where an RIS composed of passive reflecting elements is deployed on a UAV for higher mobility and better channel conditions, in the presence of innegligible interference. In addition, the very small hardware size of the RIS enables it to be effortlessly attached to walls, interior ceiling in building or even attached to UAVs. As for their flexible replacement, easy reconfiguration and costless deployment, RIS are suitable to be integrated into already existing networks.

As for D2D communications associated with RIS, it is full of challenges and research on this topic has not yet been fully investigated. This is because, in addition to direct path, there is reflected useful signal from the RIS-assisted one-hop. Accordingly, the signal of both paths are super-positioned at the receiver side to get an amplified signal with the mitigating interference attenuated as much as possible.

III. System and Channel Model

A. System Model

Consider a single cell cellular RIS-aided network as shown in Fig. 1 which consists of one mobile device (MD), one UAV, one BS and M D2D pairs that coexist and share the same frequency resources with the MD. In fact, the uplink communication link between the MD and the BS and the link between any D2D pairs are established with the assistance of a UAV equipped with an RIS. It is assumed that the MD and D2D pairs are located randomly in the xy plane, where the BS is in the yz plane. For the UAV equipped with RIS, it is also assumed to be in the yz plane. Simultaneously, the RIS is capable of supporting a number of D2D pairs that share the same frequency with the MD. Assuming the number of D2D pairs is M. Therefore, we have a total of $Q = M + 1$ links in our system. For any of those Q links, both the direct transmission link and the RIS-based reflected link are considered for the sake of enhancing the received signals. Definitely, mitigating interference exist among all links, which is a crucial issue that limits our system performance. We consider an $N \times N$ uniform planar RIS array, where it has a total of N^2 reconfigurable great quality built-in programmable elements. When there is an incident signal on the RIS, the phase shift of each of its elements is programmably tuned by varactor diodes. Accordingly, a suitable phase shift is provided by the metal plate to alleviate interference among the links and boost the system performance.

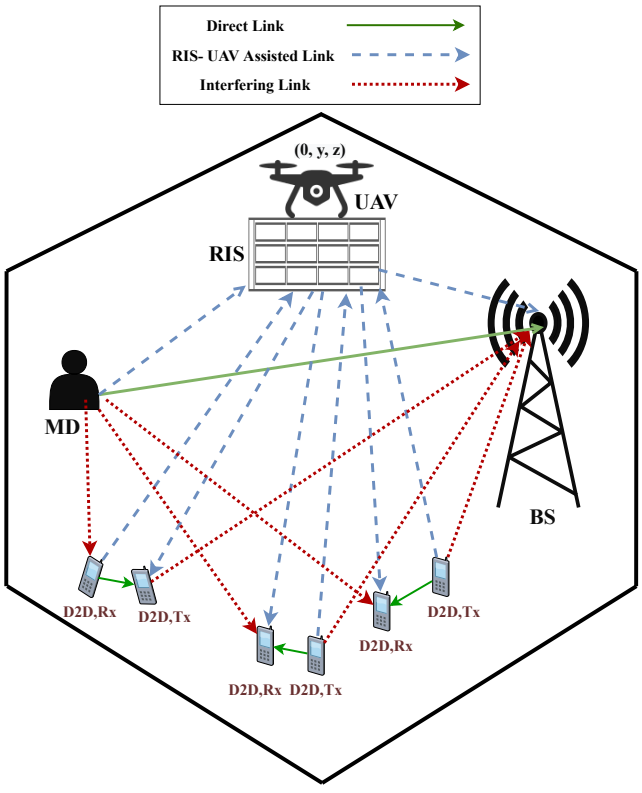

Fig. 1: Scenario under consideration where a UAV equipped with an RIS is deployed to assist the communication link between the MD and the BS as well as between D2D pairs.

In addition, we deploy this RIS on a UAV to enhance the adaptability of the system. However, just for simplicity, we assume we have a fixed-positioned UAV. The phase shift of each RIS element can take discrete values with equal quantization intervals between [0, 2π]. Assuming that the number of quantization bits is b, there exist 2^b levels of phase shift values that can be assigned to tune the RIS reconfigurable elements. The frequency response caused by any of the RIS elements given as $e^{j\theta_{y,z}}$, where the amplitude reflection coefficient of each RIS element is assigned the value 1 and $\theta_{y,z} = \frac{2L\pi}{2^b-1}$ and $L = \{0, 1, 2, ... 2^b - 1\}$. In other words, the incident signal on any RIS element is multiplied by the frequency response of this element. That is, the reflector is deployed as a virtual source that forwards the incident composite signals on each element to the intended receiver.

B. Channel Model

In the following, the THz channel model is introduced. It was mainly developed using THz wave atmospheric transmission attenuation model in addition to water vapour absorption. The LOS THz channel gain can be formulated as [18]:

$$h = \sqrt{\frac{1}{PL(f,d)}}, \tag{1}$$

where $PL(f,d)$ is the pathloss that frequency f encounters whenever traveling a distance d.

$PL(f,d)$ involves spreading loss $L_{sl}(f,d)$ and molecular absorption $L_{mal}(f,d)$ that characterizes the THz band. The spreading loss $L_{sl}(f,d)$ is due to the expansion of the electromagnetic wave while it propagates through various mediums. Nevertheless, the molecular absorption $L_{mal}(f,d)$ is a result of the collisions between atmospheric gas and/or water molecules. Detailed investigation on the effect of atmospheric attenuation was conducted in[18]. The channel coefficient h follows zero-mean complex Gaussian distribution with variance that models free space path and molecular absorption gain. From [18] (Eqn. (2), (3) and (5)), the pathloss at frequency f

when propagating a distance d is related to the variance of the THz channel and is expressed as:

$$PL(f,d) = \frac{1}{\sigma^2} = \frac{1}{G_{Tx}G_{Rx}}(\frac{4\pi fd}{c})^2 e^{k(f)d}, \tag{2}$$

where σ^2 is the variance of the THz channel with zero mean and hence, $h \sim CN(0,\sigma^2)$. G_{Tx} and G_{Rx} are the transmitter and the receiver antenna gains, c is the speed of light in free space and $k(f)$ is the frequency dependent medium absorption factor provided in [19].

IV. Mathematical Formulation

The received signal at the receiver of link i can be expressed as:

$$\begin{aligned} r_i = &\underbrace{\sqrt{P_i}X_{t_i}h_{r_i,t_i}}_{\text{useful direct signal}} + \underbrace{\sqrt{P_i}X_{t_i}\sum_{y,z} h_{y,z}^{RIS,t_i} e^{j\theta_{y,z}} h_{y,z}^{r_i,RIS}}_{\text{useful reflected signal}} \\ &+ \sum_{j\in Q, j\neq i}\Bigg\{ \underbrace{\sqrt{P_j}X_{t_j}h_{r_i,t_j}}_{\text{direct interfering signal}} + \\ &\sum_{y,z}\underbrace{\sqrt{P_j}X_{t_j}h_{y,z}^{RIS,t_j}e^{j\theta_{y,z}}h_{y,z}^{r_i,RIS}}_{\text{reflected interfering signal}}\Bigg\} + \underbrace{n_o}_{\text{AWGN}}; \end{aligned} \tag{3}$$

where P_i is the transmitting power of the transmitter t_i , X_{t_i} is the transmitting signal of transmitter t_i and has unit energy, h_{r_i,t_i} is the direct channel gain sensed at receiver r_i from the transmitting device t_i of the i_{th} link, $h_{y,z}^{RIS,t_i}$ is the $t_i - RIS$ reflected signal channel gain from the RIS element y,z, $h_{y,z}^{r_i,RIS}$ is the $RIS - r_i$ reflected signal channel gain from the RIS element y,z and n_o denotes the additive white Gaussian noise (AWGN) and has zero mean and variance N_o. For simplicity, we let $\boldsymbol{P}$ = $[P_1, P_2, ...P_Q]$ representing the transmitting powers of all transmitters from i to Q.

So, the achieved SINR for any link i is expressed as

$$\gamma_{r_i} = \frac{P_i|h_{r_i,t_i} + \sum_{y,z} h_{y,z}^{RIS,t_i} e^{j\theta_{y,z}} h_{y,z}^{r_i,RIS}|^2}{\sum_{j\in Q, j\neq i} P_j|h_{r_i,t_j} + \sum_{y,z} h_{y,z}^{RIS,t_j} e^{j\theta_{y,z}} h_{y,z}^{r_i,RIS}|^2 + N_o} \tag{4}$$

Accordingly, the corresponding achievable transmission rate of link i can be expressed, utilizing Shannon's capacity formula, as

$$\begin{aligned} R_{r_i} = Wlog_2\Bigg\{1+ \\ \frac{P_i|h_{r_i,t_i} + \sum_{y,z} h_{y,z}^{RIS,t_i} e^{j\theta_{y,z}} h_{y,z}^{r_i,RIS}|^2}{\sum_{j\in Q, j\neq i} P_j|h_{r_i,t_j} + \sum_{y,z} h_{y,z}^{RIS,t_j} e^{j\theta_{y,z}} h_{y,z}^{r_i,RIS}|^2 + N_o}\Bigg\}; \end{aligned} \tag{5}$$

where W is the system's available bandwidth.
The optimization objective is to maximize the sum rate and the optimization variables are the transmission powers of all the links, $\boldsymbol{P}$ and the phase shifts for all RIS elements $\boldsymbol{\Theta_{N\times N}}$. Assuming that the minimum required SINR for any link i is γ_{min}, the optimization problem can be formulated as:

$$\max_{\boldsymbol{P},\boldsymbol{\Theta}} \sum_{i=1}^{Q} R_{r_i}, \tag{6a}$$

$$s.t. \gamma_{r_i} \geq \gamma_{min}, \forall i = 1,2,..Q, \tag{6b}$$

$$0 < P_i < P_{max}, \forall i = 1,2,..Q, \tag{6c}$$

$$\begin{aligned} \theta_{y,z} = \frac{2\pi L}{2^b - 1} \in \boldsymbol{\Theta}_{N\times N} \\ L = 1,2,..e^b - 1, \forall y,z = 1,2,...N; \end{aligned} \tag{6d}$$

where (6b) indicates the minimum required SINR for each link to guarantee QoS and (6c) constraints the maximum power budget dedicated to each transmitter. (6d) represents the frequency responce of any RIS element, where phase shifts can take discrete values.
It is noted that the optimization problem in (6) is a mixed integer, non-convex and non-linear optimization problem. This is because both the objective function and (6b) involve non-convex SINR formula in which $\boldsymbol{P}$ and $\boldsymbol{\Theta}_{N\times N}$ are hardly coupled. Hence, this adds challenges and difficulty to the optimization problem.
To solve the optimization problem presented in (6), we decouple it into power allocation and phase shifts optimization problems assuming fixed place for the UAV. The two sub-problems are solved individually in an iterative manner.

V. Joint Power Allocation-Phase Shifts Optimization algorithm

In this section, we decouple the optimization problem presented in (6) into two sub-problems to be solved individually in an iterative manner until the algorithm converges and optimal solution is obtained. We first solve the power allocation sub-problem given fixed phase shifts for the RIS elements.

A. Power Allocation Sub-Problem Algorithm

The power allocation sub-problem given fixed phase shifts is presented as:

$$\max_{\boldsymbol{P}} \sum_{i=1}^{Q} R_{r_i}, \tag{7a}$$

$$s.t. \gamma_{r_i} \geq \gamma_{min}, \forall i = 1,2,..Q, \tag{7b}$$

$$0 < P_i < P_{max}, \forall i = 1,2,..Q, \tag{7c}$$

where the above problem is still non-convex non-linear problem with respect to $\boldsymbol{P}$. The objective function presented in (7) can be equivalently represented as:

$$\begin{aligned} \max_{\boldsymbol{P}} \sum_{i=1}^{Q} log_2\Bigg\{1+ \\ \frac{P_i|h_{r_i,t_i} + \sum_{y,z} h_{y,z}^{RIS,t_i} e^{j\theta_{y,z}h_{y,z}^{r_i,RIS}}|^2}{\sum_{j\in Q, j\neq i} P_j|h_{r_i,t_j} + \sum_{y,z} h_{y,z}^{RIS,t_j} e^{j\theta_{y,z}} h_{y,z}^{r_i,RIS}|^2 + N_o}\Bigg\} \end{aligned} \tag{8}$$

By performing common denominator and deploying basic log properties, (8) is expressed as:

$$\min_{\boldsymbol{P}} \Bigg\{ log_2\Bigg(\sum_{j\in Q, j\neq i} P_j |h_{RIS,t_j} + \sum_{y,z} h_{y,z}^{r_i,t_j} e^{j\theta_{y,z}} h_{y,z}^{r_i,RIS}|^2 + N_o \Bigg) - log_2\Bigg(\sum_{j\in Q, j\neq i} P_j |h_{r_i,t_j} + \sum_{y,z} h_{y,z}^{RIS,t_j} e^{j\theta_{y,z}} h_{y,z}^{r_i,RIS}|^2 + P_i |h_{r_i,t_i} + \sum_{y,z} h_{y,z}^{RIS,t_i} e^{j\theta_{y,z}} h_{y,z}^{r_i,RIS}|^2 + N_o \Bigg) \Bigg\}. \tag{9}$$

According to the above mathematical decomposition, the objective function in (7) is equivalent to the difference between two concave logarithmic functions denoted as $A_i(\boldsymbol{P})$ and $B_i(\boldsymbol{P})$ respectively and is given as:

$$\begin{aligned} &A_i(\boldsymbol{P}) = \\ &log_2\Bigg\{ \sum_{j\in Q, j\neq i} P_j |h_{r_i,t_j} + \sum_{y,z} h_{y,z}^{r_i,t_j} e^{j\theta_{y,z}}|^2 + N_o \Bigg\}; \\ &B_i(\boldsymbol{P}) = log_2\Bigg\{ P_i |h_{r_i,t_i} + \sum_{y,z} h_{y,z}^{r_i,t_i} e^{j\theta_{y,z}}|^2 \\ &+ P_j |\sum_{j\in Q, j\neq i} h_{r_i,t_j} + \sum_{y,z} h_{y,z}^{r_i,t_j} e^{j\theta_{y,z}}|^2 + N_o \Bigg\}. \end{aligned} \tag{10}$$

Since the rates achieved at γ_{r_i} and γ_{min} are R_{r_i} and log_2 (1 + γ_{min}), respectively and by using (7) and (10), the optimization problem can be expressed as:

$$\min_{\boldsymbol{P}} \sum_{i=1}^{Q} S_i(\boldsymbol{P}) \triangleq A_i(\boldsymbol{P}) - B_i(\boldsymbol{P}); \tag{11a}$$

$$s.t. A_i(\boldsymbol{P}) - B_i(\boldsymbol{P}) \leq -log_2(1+\gamma_{min}), \forall i = 1,2,..Q; \tag{11b}$$

$$0 \leq P_i \leq P_{max}, \forall i = 1,2,..Q; \tag{11c}$$

The optimization problem presented in (11) is now easier to solve. An iterative gradient descent method is utilized to accelerate the convergence rate of the objective function. By deploying the 2^{nd} Taylor expansion in the n^{th} iteration, $A_i(\boldsymbol{P})$ is expressed as:

$$\begin{aligned} A_i(\boldsymbol{P}) = A_i(\boldsymbol{P}^{(n)}) + \sum_{m=1}^{Q} \frac{\partial A_i(\boldsymbol{P})}{\partial P_m}|_{\boldsymbol{P}=\boldsymbol{P}^{(n)}} (P_m - P_m^{(n)}) \\ + \frac{1}{2}\sum_{m=1}^{Q} (P_m - P_m^{(n)})^T \frac{\partial^2 A_i(\boldsymbol{P})}{\partial^2 P_m}|_{\boldsymbol{P}=\boldsymbol{P}^{(n)}} (P_m - P_m^{(n)}); \end{aligned} \tag{12}$$

where n indicates the n^{th} iteration. The optimization problem can now be expressed as:

$$\min_{\boldsymbol{P}} J^{(n)}(\boldsymbol{P}); \tag{13a}$$

$$s.t. S_i^{(n)}(\boldsymbol{P}) \leq -log_2(1+\gamma_{min}), \forall i = 1,2,..Q; \tag{13b}$$

$$0 \leq P_i \leq P_{max}, \forall i = 1,2,..Q. \tag{13c}$$

where

$$J^{(n)}(\boldsymbol{P}) = \sum_{i=1}^{Q} S_i^{(n)}(\boldsymbol{P}). \tag{14}$$

Substituting with (14) in (13a), $J^{(n)}(\boldsymbol{P})$ can be expressed as:

$$\begin{aligned} J^{(n)}(\boldsymbol{P}) = \sum_{i=1}^{Q} \Bigg\{ A_i(\boldsymbol{P}^{(n)}) + \sum_{m=1}^{Q} \frac{\partial A_i(\boldsymbol{P})}{\partial P_m}|_{\boldsymbol{P}=\boldsymbol{P}^{(n)}} (P_m - P_m^{(n)}) \\ + \frac{1}{2}\sum_{m=1}^{Q} (P_m - P_m^{(n)})^T \frac{\partial^2 A_i(\boldsymbol{P})}{\partial^2 P_m}|_{\boldsymbol{P}=\boldsymbol{P}^{(n)}} (P_m - P_m^{(n)}) - B_i(\boldsymbol{P}) \Bigg\}. \end{aligned} \tag{15}$$

The solution of the power allocation sub-problem (7) is summarized in Algorithm 1. The objective function in (7b) is reformulated using some simple mathematical transformations and is expressed in (9). Accordingly, the objective function can be expressed as the difference of two concave functions. The power allocation problem is now equivalently reformulated in (11). After that, the 2^{nd} Taylor's expansion is used to approximate the non-convex original problem. So, the objective function is now expressed in (15). For P_i, the gradient descent method is deployed to get the optimal transmitting powers. σ is updated for each iteration. The optimal values for each iteration is generated using $0 < P_i < P_{max}, \forall i = 1,2...Q$. The minimum SINR, γ_{min} is checked in each iteration to guarantee a good QoS. This algorithm continues until the difference between two sum rates is less than a threshold ϵ. So, P^{opt} is obtained.

B. Discrete Phase Shift Optimization Algorithm

Now, we solve the optimization problem given in (6) given fixed transmitting powers $\boldsymbol{P}$. So, the powers constraints in (6)

Algorithm 1: Transmitting Power Allocation Sub-Problem

Initialize: n = 0 , $\sigma^{(0)} = 20, \forall i = 1,2,...Q$
Output: P^{opt}
Optimization problem (13) is solved for $P_i, i = 1,2....Q$.
Objective function $J^{(n)}(\boldsymbol{P})$ is defined in (15).
$P_i^{(n+1)} = (P_i^{(n)} - \sigma^{(n)} \frac{\partial J^{(n)}(\boldsymbol{P})}{\partial P_i}|_{P_i = P_i^{(n)}})^+$,
if $P_i^{(n+1)} > P_{max}$ **then**
  $P_i^{(n+1)} = P_{max}$;
$\sigma^{(n+1)} = \frac{\sigma_{(n)}}{2}$;
if $\gamma_i < \gamma_{min}$ **then**
  $P_i^{(n+1)} = 0$;
if $|R(\boldsymbol{P}^{(n+1)}) - R(\boldsymbol{P}^{(n)})| < \epsilon$ **then**
  $\boldsymbol{P}^{opt} = \boldsymbol{P}^{(n+1)}$; **else**
    $n = n + 1$, repeat whole algorithm

are now removed and the problem now can be represented as:

$$\max_{\mathbf{\Theta}} \sum_{i=1}^{Q} R_{r_i}, \tag{16a}$$

$$s.t. \gamma_{r_i} \geq \gamma_{min}, \forall i = 1, 2, ..Q, \tag{16b}$$

$$\theta_{y,z} = \frac{2\pi L}{2^b - 1} \in \mathbf{\Theta}_{N \times N}, \quad L = 1, 2, ..e^b - 1, \forall y, z = 1, 2, ...N, \tag{16c}$$

The objective function (16a) and the constraints (16b) and (16c) are still not convex with respect to $\mathbf{\Theta}$. In addition, $\mathbf{\Theta}$ involves a series of discrete variables depending on the RIS quantization levels L. We propose the discrete local search method to solve this problem and the exact steps are shown in Algorithm 2. Simply, for each element $\theta_{y,z}$, all possible values are traversed and the optimal one,ex: $\theta_{y,z}^{opt}$, is chosen given that the SINR constraint is satisfied, given that the other $N^2 - 1$ are kept fixed. Then, this optimal value $\theta_{y,z}^{opt}$ is used as the new value of $\theta_{y,z}^{opt}$ to optimize another phase shift, till all N^2 phase shifts in $\mathbf{\Theta}_{N \times N}$ are fully optimized. Algorithm 2 summarizes the local search algorithm for phase shifts optimization.

C. Joint Power Allocation and Phase Shifts Optimization

The joint power allocation and phase shifts optimization is summarized in Algorithm 3. In Algorithm 3, we first optimize the links' transmitting powers while the phase shift matrix is randomly generated. Then, the obtained transmitting powers are utilized in turn in the local search phase shift algorithm to generate the optimum phase shifts. Transmission powers and phase shifts are continuously updated in an alternating manner until the algorithm converges. In other words, the difference between two consecutive sum rate values is less than the convergence threshold, ϵ.

Algorithm 2: Local Search Phase Shift Algorithm

Initialize: quantization levels L
Output: $\mathbf{\Theta}_{N \times N}^{opt}$
for $y = 1 : N$ **do**
  for $z = 1 : N$ **do**
    Assign all possible values to $\theta_{y,z}$ and select the value that maximizes the sum rate, given that SINR constraint in (16b) is satisfied, ;
    $\theta_{y,z} = \theta_{y,z}^{opt}$.

Algorithm 3: Joint Power Allocation and Phase Shifts Optimization Algorithm

Initialize: $\epsilon = 10^{-3}$, $r = 0$, $P_i^{(0)} = P_{max}$, $\forall i = 1, 2, ..Q$, choose the number of quantization levels: b, randomly generate $\mathbf{\Theta}_{N \times N}$.
Given $\mathbf{\Theta}_{N \times N}$ update $\boldsymbol{P}$ using Algorithm 1.
Given P^{opt}, update $\mathbf{\Theta}_{N \times N}$ using Algorithm 2.
if $|R(\boldsymbol{P}^{(r+1)}) - R(\boldsymbol{P}^{(r)})| < \epsilon$ **then**
  $\mathbf{P}^{opt}, \mathbf{\Theta}_{N \times N}^{opt}, R_{opt}$; **else**
    $r = r + 1$, repeat whole algorithm

VI. Performance Evaluation and Numerical Results

In this section, the performance of the proposed joint power allocation and phase optimization scheme is evaluated using Matlab R2021a and compared with three other schemes. The effect of varying some parameters such as number of RIS elements N, minimum SINR γ_{min}, number of bits b and distance d on the performance of the algorithm is studied. Also, some parameters are varied and results are obtained accordingly. It is worth mentioning that the average of numerical results is taken over 20 iterations. We assume a square area for the deployment of all links with an edge of 100 m. We assume that we have three pairs of D2D devices (M = 3) and they are uniformly and randomly distributed in the xy plane in the specified square area. The BS is located in the yz plane. Also, the UAV that is equipped with the RIS is located somewhere between the MD and the BS. The values of the simulation parameters are summarized in Table I.

To prove the effectiveness of the proposed scheme, the proposed joint power allocation and phase shifts optimization is compared with the following three schemes:

- *Maximum Power Allocation (MPA)*:
  In this algorithm, the cellular and D2D links are assigned the maximum transmission power with no power allocation performed. In other words, the maximum power budget P_{max} is assigned to all links without any power optimization strategy. Only phase shifts optimization is performed to reconfigure the RIS elements and boost the sum rate somehow.
- *Random Phase Shifts (RPS)*:
  In this algorithm, random values are assigned for the phase shifts of the RIS elements. However, the power allocation algorithm is performed for the sake of getting a higher sum rate.
- *No-RIS*:
  In this algorithm, no RIS is used for signal reflection and only direct paths are received at each receiving node. Only power allocation algorithm is applied.

In Fig. 2, the number of quantization levels is set to 3. The sum rate of the proposed scheme, MPA, RPS and no–RIS are plotted versus the number of RIS elements N. The figure shows

TABLE I: Simulation Parameters.

Parameter	Description	Value
f	Operating Frequency	1 THz
$k(f)$	Absorption Coefficient	0.1
P_{max}	Power Budget	0.2 W
N_o	Noise Variance	-170 dBm
W	Available BW	10^8 Hz
γ_{min}	Minimum SINR	0.1
ϵ	Convergence Threshold	10^{-3}

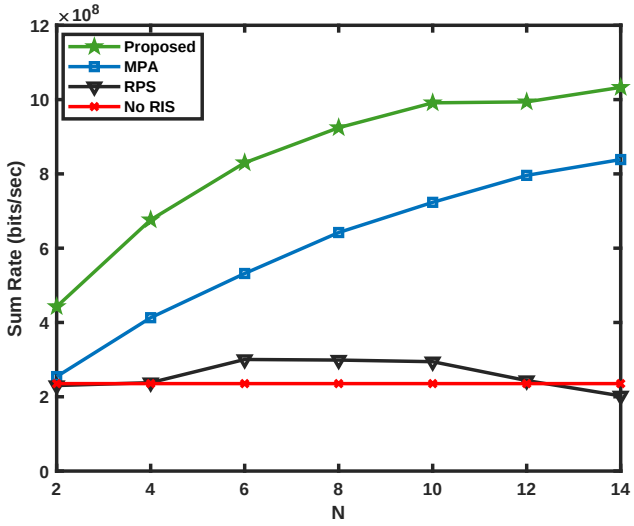

Fig. 2: Sum rate versus number of RIS elements N.

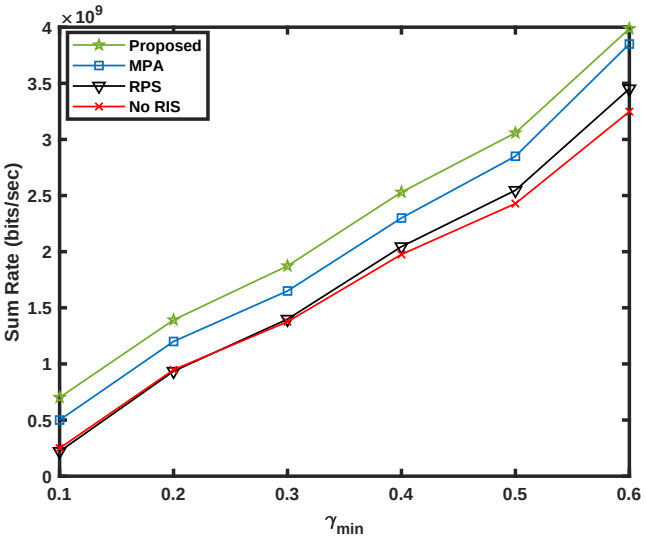

Fig. 4: Sum rate versus minimum SINR γ_{min}.

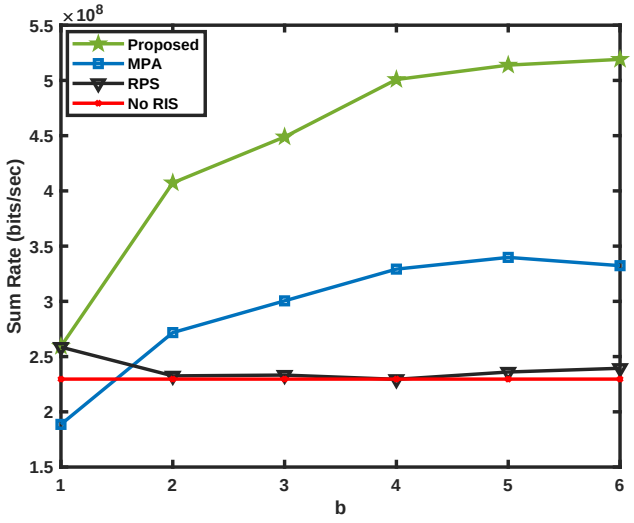

Fig. 3: Sum rate versus the number of bits b.

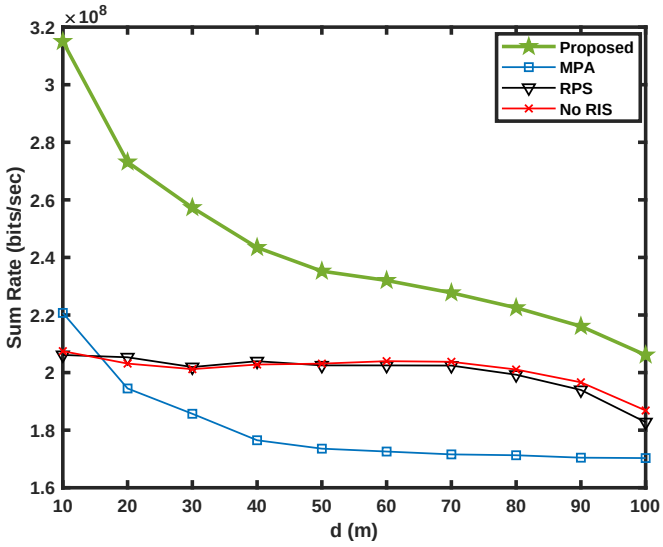

Fig. 5: Sum rate versus distance between each two communicating nodes.

that the performance of the proposed scheme is found superior over the considered range of N compared to the other three schemes. Moreover, the sum rate achieved by the proposed scheme and that of the MPA increases as N increases. This in turn proves the effectiveness of applying passive RIS-assisted network so that undesired channel mitigation can be eliminated. Moreover, it is noticed that at N = 12, increasing N slightly contributes in increasing the sum rate of the proposed scheme and MPA. This is expected since increasing N over a certain value results in an increase in the number of interfering signals. For the RPS, increasing the number of elements N results in increasing the interference remarkably since no phase shift optimization is performed, instead phase shifts are randomly selected. So, the sum rate is slightly increasing from N = 2 to N = 6. Then, it is almost constant from N = 6 to N = 10. After that, the curve decreases when N exceeds 10. The worst performance among the 4 schemes is provided by the No–RIS scheme which illustrates the effectiveness of deploying an RIS in the network.

In Fig. 3, the sum rate of the proposed scheme along with that achieved by MPA, RPS and No-RIS are plotted versus the number of bits b. It is shown from the figure that the proposed scheme achieves the highest sum rate among the three other schemes over the whole range of b. In addition, it is noted that the sum rate obtained from both the proposed scheme and the MPA increases significantly as long as b increases, till $b = 4$. Then, their sum rate changes with a very small rate compared to that obtained from $b = 1$ to $b = 4$. For the RPS, the sum rate obtained encounters a decrease from $b = 1$ to

$b = 2$, then remains almost constant from $b = 2$ to $b = 4$. After that, it again increases from $b = 5$ to $b = 6$. This is due to the random phase shifts values assigned to the RIS elements that are selected in a random manner. Accordingly, RPS encounter fluctuations along the range of b. The No-RIS achieves constant sum rate.

Fig.4 shows the achieved sum rate versus the minimum required SINR γ_{min} for $N = 5$ for the four schemes. It is observed that as long as γ_{min} increases, the sum rate achieved by each scheme increases. This is expected since improving the lower bound of the network constraint γ_{min}, the system performance is accordingly improved. Also, the proposed scheme has the highest achieved sum rate, followed by MPA, RPS and No-RIS. This proves the high adaptability of the proposed scheme compared to the other considered schemes. This is because the transmitting powers and the phase shifts of the RIS elements are optimized for the sake of maximizing the sum rate.

In Fig.5, the distance between all communicating nodes is adjusted and denoted as d. So, the achieved sum rate of the four schemes is plotted versus d, where d ranges from 10 m to 100 m. As the figure depicts, increasing the distance between each two communicating nodes results in a degradation in the achieved sum rate. This is due to the higher pathloss that the propagating signal encounters when travelling a longer distance, which is considered as one of the challenges of THz communications. Furthermore, the proposed scheme achieves the highest sum rate among the three schemes, followed by RPS and No-RIS which almost have the same performance. The worst sum rate among other schemes is obtained by the MPA scheme, which proves the inefficiency of this scheme especially at long distances.

VII. Conclusions and Future

In this paper, the sum rate of an uplink RIS-aided network involving one cellular user and a number of D2D users, where the RIS is positioned on a UAV, in THz is derived. The RIS-reflected paths as well as direct paths between each two communicating nodes is considered. The maximization of the derived sum rate is considered, where the transmitting powers as well as the phase shifts of the RIS elements are optimized separately. Then, a joint power allocation and phase shifts optimization problem is formulated and solved using gradient descent method, Taylor's expansion and local search method for the phase shifts. The performance of the proposed joint power allocation and phase shifts optimization problem has been compared with three other schemes. The results show that sum rate using the obtained optimum powers and the optimum phase shifts is significantly higher than that of the other three schemes. It is noted that, the obtained optimum powers of the proposed algorithm as well as the phase shifts of the RIS elements are adaptive and change according to the number of users, minimum SINR required and number of bits b utilized. For future works, the dynamic positioning for the UAV and analyzing the sum rate in the context of re-positioning the RIS-equipped UAV is to be investigated.

References

[1] F. Shi, W. Wang, H. Wang, and H. Ning, "The internet of people: A survey and tutorial," *arXiv preprint arXiv:2104.04079*, 2021.

[2] H. Elayan, O. Amin, R. M. Shubair, and M.-S. Alouini, "Terahertz communication: The opportunities of wireless technology beyond 5g," in *2018 International Conference on Advanced Communication Technologies and Networking (CommNet)*. IEEE, 2018, pp. 1–5.

[3] M. H. Alsharif, A. H. Kelechi, M. A. Albreem, S. A. Chaudhry, M. S. Zia, and S. Kim, "Sixth generation (6g) wireless networks: Vision, research activities, challenges and potential solutions," *Symmetry*, vol. 12, no. 4, p. 676, 2020.

[4] Y. Amarasinghe, W. Zhang, R. Zhang, D. M. Mittleman, and J. Ma, "Scattering of terahertz waves by snow," *Journal of Infrared, Millimeter, and Terahertz Waves*, vol. 41, no. 2, pp. 215–224, 2020.

[5] R. Singh and D. Sicker, "Beyond 5g: Thz spectrum futures and implications for wireless communication," 2019.

[6] M. H. Zafar, I. Khan, and M. O. Alassafi, "An efficient resource optimization scheme for d2d communication," *Digital Communications and Networks*, 2022.

[7] Z. Ji, Z. Qin, and C. G. Parini, "Reconfigurable intelligent surface aided cellular networks with device-to-device users," *IEEE Transactions on Communications*, vol. 70, no. 3, pp. 1808–1819, 2022.

[8] Y. Chen, B. Ai, H. Zhang, Y. Niu, L. Song, Z. Han, and H. V. Poor, "Reconfigurable intelligent surface assisted device-ttitleo-device communications," *IEEE Transactions on Wireless Communications*, vol. 20, no. 5, pp. 2792–2804, 2020.

[9] W. Long, R. Chen, M. Moretti, W. Zhang, and J. Li, "A promising technology for 6g wireless networks: Intelligent reflecting surface," *Journal of Communications and Information Networks*, vol. 6, no. 1, pp. 1–16, 2021.

[10] S. Farrag, E. Maher, A. El-Mahdy, and F. Dressler, "Performance analysis of UAV assisted mobile communications in THz channel," *IEEE Access*, vol. 9, pp. 160 104–160 115, Dec. 2021.

[11] A. Gupta and R. K. Jha, "A survey of 5G network: Architecture and emerging technologies," *IEEE Access*, vol. 3, pp. 1206–1232, May 2015.

[12] S. K. Khan, A. Al-Hourani, and K. G. Chavez, "Performance evaluation of amplify-and-forward uav relay in millimeter-wave," in *2020 27th International Conference on Telecommunications (ICT)*. IEEE, 2020, pp. 1–5.

[13] L. Yang, J. Yang, W. Xie, M. O. Hasna, T. Tsiftsis, and M. Di Renzo, "Secrecy performance analysis of ris-aided wireless communication systems," *IEEE Transactions on Vehicular Technology*, vol. 69, no. 10, pp. 12 296–12 300, 2020.

[14] Q. N. Le, V.-D. Nguyen, O. A. Dobre, and R. Zhao, "Energy efficiency maximization in ris-aided cell-free network with limited backhaul," *IEEE Communications Letters*, vol. 25, no. 6, pp. 1974–1978, 2021.

[15] Y. Pan, K. Wang, C. Pan, H. Zhu, and J. Wang, "Uav-assisted and intelligent reflecting surfaces-supported terahertz communications," *IEEE Wireless Communications Letters*, vol. 10, no. 6, pp. 1256–1260, 2021.

[16] Z. Guan and T. Kulkarni, "On the effects of mobility uncertainties on wireless communications between flying drones in the mmwave/thz bands," in *IEEE INFOCOM 2019-IEEE Conference on Computer Communications Workshops (INFOCOM WKSHPS)*. IEEE, 2019, pp. 768–773.

[17] S. Farrag, E. Maher, A. El-Mahdy, and F. Dressler, "Outage probability analysis of UAV assisted mobile communications in THz channel," in *16th IEEE/IFIP Conference on Wireless On demand Network Systems and Services (WONS 2021)*. Virtual Conference: IEEE, Mar. 2021.

[18] A.-A. A. Boulogeorgos, E. N. Papasotiriou, and A. Alexiou, "A distance and bandwidth dependent adaptive modulation scheme for thz communications," pp. 1–5, 2018.

[19] J. M. Jornet and I. F. Akyildiz, "Channel Modeling and Capacity Analysis for Electromagnetic Wireless Nanonetworks in the Terahertz Band," *IEEE Transactions on Wireless Communications (TWC)*, vol. 10, no. 10, pp. 3211–3221, Oct. 2011.